

# Crack resistance by interfacial bridging: Its role in determining strength characteristics

Robert F. Cook

IBM, Thomas J. Watson Research Center, Yorktown Heights, New York 10598

Carolyn J. Fairbanks, Brian R. Lawn, and Yiu-Wing Mai<sup>a)</sup>

Ceramics Division, National Bureau of Standards, Gaithersburg, Maryland 20899

(Received 27 October 1986; accepted 3 March 1987)

An indentation-strength formulation is presented for nontransforming ceramic materials that show an increasing toughness with crack length (T curve, or R curve) due to the restraining action of interfacial bridges behind the crack tip. By assuming a stress-separation function for the bridges a microstructure-associated stress intensity factor is determined for the penny-like indentation cracks. This stress intensity factor opposes that associated with the applied loading, thereby contributing to an *apparent* toughening of the material, i.e., the measured toughness in excess of that associated with the intrinsic cohesion of the grain boundaries (intergranular fracture). The incorporation of this additional factor into conventional indentation fracture mechanics allows the strengths of specimens with Vickers flaws to be calculated as a function of indentation load. The resulting formulation is used to analyze earlier indentation-strength data on a range of alumina, glass-ceramic, and barium titanate materials. Numerical deconvolution of these data determines the appropriate T curves. A feature of the analysis is that materials with pronounced T curves have the qualities of flaw tolerance and enhanced crack stability. It is suggested that the indentation-strength methodology, in combination with the bridging model, can be a powerful tool for the development and characterization of structural ceramics, particularly with regard to grain boundary structure.

## I. INTRODUCTION

Recent studies have shown that many polycrystalline, non-phase-transforming ceramics exhibit an increasing resistance to crack propagation with crack length.<sup>1-8</sup> At small flaw sizes, comparable to the scale of the microstructure, the toughness  $T$  is an intrinsic quantity representative of the weakest fracture path. At large flaw sizes the toughness tends to a higher, steady-state value representative of the cumulative crack/microstructure interactions in the polycrystal. The progressive transition from the low-to-high toughness limits during crack extension is described as the T curve. [The concepts of T curve and R curve are equivalent.<sup>9</sup> In the former the equilibrium condition is obtained by equating the net stress intensity factor  $K$ , characterizing the net applied load on the crack, to the toughness  $T$  (alternatively designated  $K_{IC}$  in some of the earlier literature) characterizing critical crack resistance forces. In the latter, the mechanical energy release rate  $G$ , derived from the work done by the applied loading during crack extension, is equated to the energy necessary to create the fracture surfaces  $R$ .]

Perhaps the most comprehensive studies of this T-curve behavior have been made using a controlled flaw technique,<sup>1-4</sup> in which the strengths of specimens containing indentations are measured as a function of indentation load. It was found that, for large flaws, the strengths tend to an "ideal"  $-\frac{1}{3}$  power law dependence of strength on indentation load, indicative of a nonvarying toughness. At small flaw sizes, however, the strengths decrease markedly from this ideal behavior, tending instead to a load-independent plateau. Significantly, in a group of polycrystalline alumina materials it was found that the strengths at large flaw sizes were all greater than those of single-crystal sapphire, whereas the reverse tended to be true at small flaw sizes.<sup>1</sup> Taken with the observation that the fracture in these aluminas is intergranular, these results suggest that the grain boundaries are paths of weakness but that there is some mechanism operating that more than compensates for this intrinsic weakness as the flaw size increases. Moreover, the strength-load responses of the polycrystalline materials themselves, even those with similar grain sizes, tended to cross each other.<sup>1</sup> It would appear that the nature of the grain boundary, as well as the grain size, influences the fracture behavior.

Two other sets of experiments provide vital clues as to the mechanism of crack/microstructure interaction

<sup>a)</sup> On leave from the Department of Mechanical Engineering, University of Sydney, New South Wales 2006, Australia.

underlying the T-curve behavior. In the first set, Knehans and Steinbrech<sup>6</sup> propagated large cracks in alumina using the single-edge-notched beam geometry. They observed strongly rising T-curves as cracks propagated from the tip of the notch. However, when interfacial material was removed from behind the crack tip by careful sawing, the toughness did not continue up the T curve but reverted to its original level, implying that the critical mechanism must be operating in the “wake” of the crack tip. In the second set of experiments, Swanson *et al.*<sup>8</sup> observed crack propagation in alumina using both indented-disk and tapered-cantilever beam specimens. Active grain-localized “bridges” were observed at the primary crack interface, over a “zone length” of millimeter scale. The implication here is that interfacial bridging ligaments *behind* the tip are providing a restraining influence on crack extension. The reversion to the base of the T curve in the experiments of Knehans and Steinbrech may be interpreted in terms of the removal of these restraining ligaments.

Mai and Lawn<sup>10</sup> developed a fracture mechanics model for the propagation of ligamentary bridged cracks, incorporating parameters characterizing the interbridge spacing, the intrinsic intergranular toughness, and the force-extension “law” for the bridges. They applied the model to the propagation of full-scale cracks propagating under double cantilever loading and thereby demonstrated consistency with the measured T-curve response in a polycrystalline alumina.

Here we shall apply the Mai–Lawn bridging model to the mechanics of the indentation-strength test. It is appropriate to do this for two reasons. First, indentation cracks are strongly representative of the small “natural” flaws that control the strengths of ceramic materials in service.<sup>1</sup> Second, and most important, the indentation methodology will be seen to be ideally suited to quantitative analysis of the T-curve function. For this purpose, recourse will be made to several earlier sources of indentation-strength data, covering a broad spectrum of ceramic materials.<sup>1,3,4,11</sup> The consequent manner in which the indentation-strength test highlights one of the most important manifestations of T-curve behavior, namely flaw tolerance, will emerge as a uniquely appealing feature of the approach. The potential for using the attendant parametric evaluations in the T-curve analysis as a tool for investigating the role of chemical composition and processing variables as determinants of toughness properties is indicated.

## II. INTERFACIAL CRACK RESTRAINT MODEL

An earlier fracture mechanics model<sup>10</sup> for straight-fronted cracks restrained by interfacial bridging ligaments is reproduced here in modified form, appropriate to penny-like indentation cracks.

## A. Equilibrium crack propagation

A fracture system is in equilibrium when the forces driving the crack extension are equal to the forces resisting this extension. Equilibria may be stable or unstable, depending on the crack-length dependence of these forces.<sup>9</sup> Here we shall characterize the driving forces by stress intensity factors  $K(c)$  and the fracture resistance by toughness  $T(c)$ , where  $c$  is the crack size. We may consider separately the stress intensity factor arising from the applied loading  $K_a$ , which is directly monitored, from that associated with any internal forces intrinsic to the microstructure  $K_i$ , such as the ligamentary bridging forces we seek to include here. We may then conveniently regard the fracture resistance of the material as the sum of an intrinsic interfacial toughness of the material  $T_0$  and the internal  $K_i$  terms.<sup>9</sup> Hence our condition for equilibrium may be written

$$K_a(c) = T(c) = T_0 - \sum_i K_i(c), \quad (1)$$

where we have summed over all internal contributions. We emphasize that  $T_0$  is strictly independent of crack length. The quantity  $T(c)$  is the effective toughness function, or T curve, for the material. To obtain a rising T curve, i.e., an increase in toughness with crack length, the sum over the  $K_i(c)$  terms must be either positive decreasing or negative increasing. In terms of Eq. (1) the condition for stability is that  $dK_a/dc < dT/dc$  and for instability  $dK_a/dc > dT/dc$ .<sup>9</sup> We see then that a rising T curve, where  $dT/dc \geq 0$ , will lead to increased stabilization of the crack system.

## B. Microstructure-associated stress intensity factor

We seek now to incorporate the effect of restraining ligaments behind the growing crack tip into a microstructure-associated stress intensity factor,  $K_\mu = \sum_i K_i$ . In the context of indentation flaws we shall develop the analysis for cracks of half-penny geometry.

A schematic model of the proposed system is shown in Fig. 1. The interfacial bridging ligaments are represented as an array of force centers,  $F(r)$ , projected onto the crack plane. Here  $c$  is the radius of the crack front and  $d$  is the characteristic separation of the centers. At very small cracks sizes,  $c < d$ , the front encounters no impedance. As the front expands, bridges are activated in the region  $d \leq r \leq c$ . These bridges remain active until, at some critical crack size  $c^* (\geq d)$ , ligamentary rupture occurs at those sites most distant behind the front. Thereafter a steady-state annular zone of width  $c^* - d$  simply expands outward with the growing crack.

The qualitative features of the crack response observed by Swanson *et al.*<sup>8</sup> would appear to be well described by the above configuration. Enhanced crack sta-

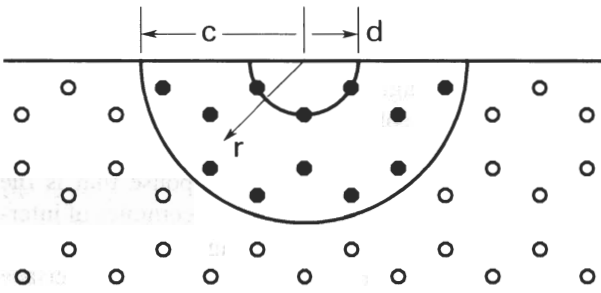


FIG. 1. Schematic diagram of a half-penny, surface crack propagating through a material with bridging ligaments impeding the crack motion. Here  $d$  is the mean ligament spacing,  $c$  is the crack radius, and  $r$  is the radial coordinate from the penny origin;  $\bullet$  denotes the active ligament sites and  $\circ$  denotes potential ligament sites.

bility arises from the increasing interfacial restraint as more and more bridging sites are activated by the expanding crack front (the number of active bridges will increase approximately quadratically with the crack radius). The discontinuous nature of the crack growth follows from the discreteness in the spatial distribution of the closure forces in the crack plane. Thus we imagine the crack to become trapped at first encounter with the barriers. If these barriers were to be sufficiently large the crack front could be "trapped" such that, at an increased level of applied stress, the next increment of advance would occur unstably to the second set of trapping sites. Further increases in applied stress would lead to repetitions of this trapping process over successive barriers, the jump frequency increasing as the expanding crack front encompasses more sites. There must accordingly be a smoothing out of the discreteness in the distribution of interfacial restraints as the crack grows until, at very large crack sizes, the distribution may be taken as continuous. With regard to the steady-state zone width ( $c^* - d$ ) referred to above, our own observations and those of Swanson *et al.*<sup>8,12</sup> indicate that, for a given material, there is a characteristic distance behind the crack tip that contains apparently intact bridges.

In principle, we should be able to write down an appropriate stress intensity factor for any given distribution of discrete restraining forces of the kind depicted in Fig. 1. However, an exact summation becomes intractable as the number of active restraining elements becomes large. To overcome this difficulty we approximate the summation over the discrete force elements  $F(r)$  by an integration over continuously distributed stresses  $\sigma(r) \approx F(r)/d^2$ . We plot these stresses for three crack configurations in Fig. 2. These stresses have zero value in the region  $r < d$ , reflecting the necessary absence of restraint prior to the intersection of the crack front with the first bridging sites. They have nonzero

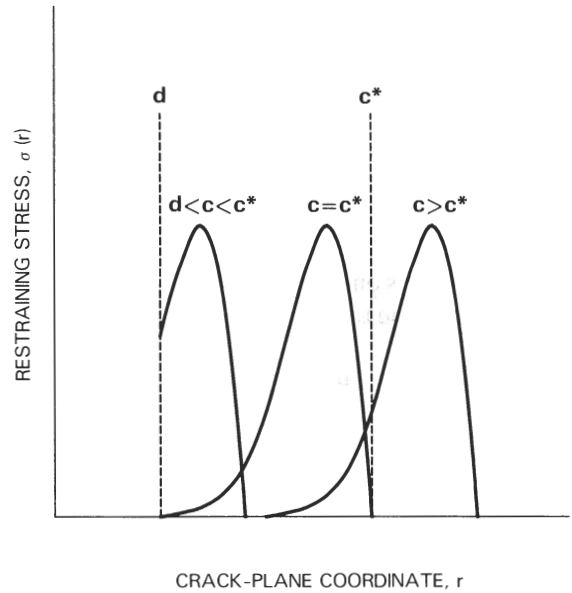


FIG. 2. Stress distribution applied by the restraining ligaments over the crack plane as a function of radial distance from the center of the crack. Note that the stress is zero for  $r < d$  and reaches a steady-state distribution for  $c > c^*$ .

value in the region  $d < r < c$  up to the crack size at which ligamentary rupture occurs ( $d \leq c \leq c^*$ ) and thereafter in the region  $d + c - c^* < r < c$ , where a steady-state configuration is obtained ( $c > c^*$ ). This approximation is tantamount to ignoring all but the first of the discontinuous jumps in the observed crack evolution. We might consider such a sacrifice of part of the physical reality to be justifiable in those cases where the critical crack configuration encompasses many bridging sites, as perhaps in a typical strength test.

The problem may now be formalized by writing down a microstructure-associated stress intensity factor in terms of the familiar Green's function solution for penny-like cracks<sup>13</sup>:

$$K_{\mu} = 0 \quad (c < d), \quad (2a)$$

$$K_{\mu} = - \left( \frac{\psi}{c^{1/2}} \right) \int_d^c \sigma(r) r \frac{dr}{(c^2 - r^2)^{1/2}} \quad (d \leq c \leq c^*), \quad (2b)$$

$$K_{\mu} = - \left( \frac{\psi}{c^{1/2}} \right) \int_{d+c-c^*}^c \sigma(r) r \frac{dr}{(c^2 - r^2)^{1/2}} \quad (c > c^*), \quad (2c)$$

where  $\psi$  is numerical crack geometry term. At this point another major difficulty becomes apparent. We have no basis, either theoretical or experimental, for specifying *a priori* what form the closure stress function  $\sigma(r)$  must take. On the other hand, we do have some feeling from the observations of Swanson *et al.*, albeit limited, as to the functional form  $\sigma(u)$ , where  $u$  is the crack opening displacement. Further, it is  $\sigma(u)$  rather than  $\sigma(r)$  that

is the more fundamental bridging quantity and that is more amenable to independent specification. Thus, given a knowledge of the crack profile, we should be able to replace  $r$  by  $u$  as the integration variable in Eq. (2) and thereby proceed one step closer to a solution.

However, even this step involves some uncertainty, as the crack profile itself is bound to be strongly influenced by the distribution of surface tractions, i.e.,  $u(r)$  strictly depends on  $\sigma(r)$  (as well as on the applied loading configuration), which we have just acknowledged as an unknown. A rigorous treatment of this problem involves the solution of two coupled nonlinear integral equations, for which no analytical solutions are available.<sup>14</sup> We thus introduce a simplification by neglecting any effect the tractions might have on the shape of the crack profile, while taking account of these tractions through their influence on the net driving force  $K = K_a + K_\mu$  from Eq. (1), in determining the magnitude of the crack opening displacements. Accordingly, we choose Sneddon's solution<sup>15</sup> for the near-field displacements of an equilibrium crack, i.e.,  $K = T_0$ ,

$$u(r,c) = (\psi T_0 / E c^{1/2})(c^2 - r^2)^{1/2}, \quad (3)$$

where  $E$  is the Young's modulus. Substitution of Eq. (3) into Eq. (2) then gives

$$K_\mu = 0 \quad (c < d), \quad (4a)$$

$$K_\mu = -\left(\frac{E}{T_0}\right) \int_0^{u(d,c)} \sigma(u) du \quad (d \leq c \leq c^*), \quad (4b)$$

$$K_\mu = -\left(\frac{E}{T_0}\right) \int_0^{u^*} \sigma(u) du \quad (c > c^*). \quad (4c)$$

We note that  $u^* = u(d, c^*)$  is independent of  $c$  so  $K_\mu$  cuts off at  $c \geq c^*$ .

Let us note here that our choice of the Sneddon profile, Eq. (3) leads us to an especially simple solution for  $K_\mu$  in Eq. (4). In particular, we note that this term is conveniently expressible as an integral of the surface closure stress as a function of the crack opening displacement, i.e., a work of separation term. This simple solution obtains *only* with the Sneddon profile. It might be argued that a Dugdale-type profile<sup>16</sup> is more appropriate, but it can be shown that the fracture mechanics are not too sensitive to the actual profile chosen.<sup>17</sup> Our main objective here is to emphasize the physical variables involved. Thus by sacrificing self-consistency in our solutions, we have obtained simple working equations for evaluating the microstructure-associated stress intensity factor. We have only to specify the stress-separation function  $\sigma(u)$ .

### C. Stress-separation function for interfacial bridges

The function  $\sigma(u)$  is determined completely by the micromechanics of the ligamentary rupture process. We have indicated that we have limited information on

what form this function should take. Generally,  $\sigma(u)$  must rise from zero at  $u = 0$  to some maximum and then decrease to zero **again at some** characteristic rupture separation  $u^*$ . The observations of crack propagation in alumina by Swanson *et al.* suggest that it is the decreasing part of this stress-separation response that is the most dominant in the polycrystalline ceramics of interest here.<sup>8</sup> The stable crack propagation observed by those authors has much in common with the interface separation processes in concrete materials that are often described by tail-dominated stress-separation functions.

The stress-separation function chosen is<sup>10</sup>

$$\sigma(u) = \sigma^*(1 - u/u^*)^m \quad (0 \leq u \leq u^*), \quad (5)$$

where  $\sigma^*$  and  $u^*$  are limiting values of the stress and separation, respectively, and  $m$  is an exponent. We consider three values of  $m$ :  $m = 0$  is the simplest case of a uniformly distributed stress acting over the annular activity zone;  $m = 1$  corresponds to simple, constant-friction pullout of the interlocking ligamentary grains;  $m = 2$  is the value adopted by the concrete community (equivalent to a decreasing frictional resistance with increasing pullout). As we shall see, the choice of  $m$  will not be too critical in our ability to describe observed strength data. Note that the representation of the stress-separation function by Eq. (5) is an infinite modulus approximation in that it totally neglects the rising part of the  $\sigma(u)$  response.

Equation (5) may now be substituted into Eq. (4) to yield, after integration,

$$K_\mu = 0 \quad (c < d), \quad (6a)$$

$$K_\mu = -(T_\infty - T_0)(1 - \{1 - [c^*(c^2 - d^2)/c(c^2 - d^2)]^{1/2}\}^{m+1}) \quad (d \leq c \leq c^*), \quad (6b)$$

$$K_\mu = -(T_\infty - T_0) \quad (c > c^*), \quad (6c)$$

where we have eliminated the stress-separation parameters  $\sigma^*$  and  $u^*$  in favor of those characterizing steady-state crack propagation,  $c^*$  and  $T_\infty$ :

$$c^* = 2(Eu^*/\psi T_0)^2 \{1 + [1 + 4(\psi T_0 d^{1/2}/Eu^*)^4]^{1/2}\} \quad (7)$$

and

$$T_\infty = T_0 + E\sigma^*u^*/(m+1)T_0. \quad (8)$$

These latter parameters are more easily incorporated into the strength analysis to follow.

A useful quantity is the work necessary to rupture an individual ligament. This work is a composite measure of the maximum sustainable stress and maximum range of the stress-extension function of Eq. (5) and is given by the area under the stress-separation curve  $\sigma(u)$ . We may express this area as

$$\Gamma_l = \int_0^{u^*} \sigma(u) du = \frac{\sigma^*u^*}{(m+1)}. \quad (9a)$$

It is useful to compare this quantity with the intrinsic interfacial energy<sup>9</sup>

$$\Gamma_0 = T_0^2/2E. \quad (9b)$$

The  $\Gamma$  terms in Eq. (9) are related, through Eq. (8), by the ratio

$$\Gamma_l/\Gamma_0 = 2(T_\infty - T_0)/T_0, \quad (10)$$

which may conveniently be regarded as a toughening index.

#### D. Strength-indentation load relations

We are now in the position to consider the mechanics of a test specimen containing an indentation crack produced at load  $P$  and subsequently subjected to an applied stress  $\sigma_a$ . To obtain the "inert strength"  $\sigma_m$ , we need to determine the equilibrium instability configuration at which the crack grows without limit.

In indentation crack systems the stress intensity factor associated with the residual contact stresses  $K_r$  augments the stress intensity factor associated with the applied loading  $K_a$  effectively giving rise to a *net* applied stress intensity factor  $K'_a$ .<sup>18,19</sup> Equation (1) becomes

$$K'_a = K_a + K_r = T(c) \\ = \psi\sigma_a c^{1/2} + \chi P/c^{3/2} = T_0 - K_\mu(c), \quad (11)$$

where  $\chi$  measures the intensity of the residual field. We note that  $K_r$  is inverse in crack size and hence will further stabilize the fracture evolution.<sup>19</sup> The indentation load determines the initial crack size at  $\sigma_a = 0$ , but *because* of the stabilization in the growth we should not necessarily expect this initial size to be an important factor in the fracture mechanics. Our problem then is to combine Eqs. (6) and (11) and invoke the instability condition  $dK'_a/dc \geq dT/dc$  to determine the strength as a function of indentation load.

Unfortunately, it is not possible to obtain closed form solutions to this problem. Limiting solutions *can* be obtained analytically, however, and we consider these first.

(i) *Small cracks (low P)*. In the region  $c \ll d$  we revert to the ideal case of zero microstructural interaction, such that Eq. (6a) applies. In this region it can be readily shown that the equilibrium function  $\sigma_a(c)$  obtained by rearranging Eq. (11) passes through a maximum, up to which point the crack undergoes stable growth.<sup>19</sup> This maximum therefore defines the instability point  $d\sigma_a/dc = 0$  (equivalent to the condition  $dK'_a/dc = dT/dc = 0$  here):

$$\sigma_m^0 = 3T_0^{4/3}/4^{4/3}\psi(\chi P)^{1/3}. \quad (12)$$

The region of validity of this solution is indicated as region I in Fig. 3.

(ii) *Large cracks (high P)*. In the region  $c \gg c^*$ , Eq. (6c) applies and we have maximum microstructural in-

teraction. The procedure to a solution is entirely the same as in the previous case, except that now  $T_\infty$  replaces  $T_0$  in Eq. (12). Thus

$$\sigma_m^\infty = 3T_\infty^{4/3}/4^{4/3}\psi(\chi P)^{1/3}. \quad (13)$$

This solution applies in region III in Fig. 3.

It is for intermediate cracks, region II in Fig. 3, that analytical solutions are difficult to obtain. Here numerical procedures will be required, but the route is nevertheless the same as before; determine  $\sigma_a(c)$  from Eq. (11) in conjunction with Eq. (6b) and apply the instability condition, taking account of the increased stabilization arising from the  $K_\mu$  term. To proceed this way we must first determine the values of the parameters in Eqs. (6) and (11). We address this problem in the next section.

### III. DERIVATION OF T CURVE FROM INDENTATION STRENGTH DATA

#### A. Crack geometry and elastic/plastic contact parameters

Our first step towards a complete parametric evaluation of the  $\sigma_m(P)$  data is to seek *a priori* specifications of the dimensionless quantities  $\psi$  and  $\chi$  in Eq. (11). The parameter  $\psi$  is taken to be material independent, since it is strictly a crack geometry term. The parameter  $\chi$  does depend on material properties, however, relating as it does competing elastic and plastic processes in the indentation contact.<sup>13</sup> We note that these parameters do not appear in the microstructural term  $K_\mu$  in Eq. (6), so ideally we can "calibrate" them from

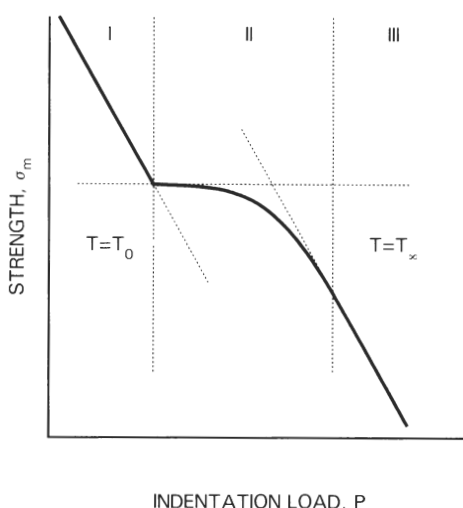


FIG. 3. Schematic strength versus indentation load plot incorporating the influence of bridging ligaments into the crack propagation response (logarithmic coordinates). The solid line represents the general solution [Eqs. (6) and (11)]. The dashed lines represent asymptotic solutions obtained analytically for small cracks [region I, Eq. (12)] and large cracks [region III, Eq. (13)].

tests on materials that do *not* exhibit T-curve behavior. The details of such calibrations are given in the Appendix. The values we use are  $\psi = 1.24$  and  $\chi = 0.0040 (E/H)^{1/2}$ , where  $H$  is the hardness.

### B. Bounding parameters for the regression procedure

We have indicated that solutions for region II of the strength-load response of Fig. 3 must be obtained numerically. Here we shall outline the regression procedure used to deconvolute the T curve for a given set of  $\sigma_m(P)$  data.

To establish reasonable first approximations for a search/regression procedure, we note two experimental observations. The first is from the indentation/strength data of Cook *et al.*<sup>1</sup> In a number of materials the  $\sigma_m(P)$  data tended strongly to the asymptotic limit of region III at large indentation loads (Fig. 3), reflecting the upper, steady-state toughness  $T_\infty$  [see Eq. (13)]. No analogous transition corresponding to  $T_0$ -controlled strengths in region I was observed: at low indentation loads the strength data were truncated by failures from natural flaws. Notwithstanding this latter restriction, we may use Eqs. (12) and (13) (with calibrated values of  $\psi$  and  $\chi$  from Sec. III A) to set upper bounds to  $T_0$  and lower bounds to  $T_\infty$  from strength data at the extremes of the indentation load range. We expect from the observations of Cook *et al.* that the lower bound estimate of  $T_\infty$  probably lies closer to the true value than the upper bound estimate to  $T_0$ .

The second experimental observation is from the crack propagation work of Swanson *et al.*,<sup>8</sup> who estimated the average distance between bridging sites at 2–5 grain diameters. We accordingly take the lower bound estimate for the interligament spacing  $d$  at 1 grain diameter. Similar bounding estimates for  $c^*$  are more difficult, although the condition  $c^* > d$  must be satisfied.

There is one further parameter we have to specify, and that is the exponent of the ligament stress-extension function  $m$ . We have alluded to the fact that the observations of Swanson *et al.* indicate that a stabilizing, tail-dominated stress-separation function should be appropriate, with  $m \geq 1$  in Eq. (5).

### C. Regression procedure

With the first approximations thus determined we search for the set of parameters for each set of  $\sigma_m(P)$  data. The scheme adopted to do this is as follows.

(1) The T curve is set from Eqs. (1) and (6) and the equilibrium  $\sigma_a(c)$  response is calculated from Eq. (11) at each indentation load for which there are *measured* strength data.

(2) The *predicted* strength at each indentation load is determined numerically from the instability require-

ment  $d\sigma_a/dc = 0$  (with the proviso that if more than one maximum in the  $\sigma_a(c)$  function exists, it is the greater that determines the strength—see Sec. IV).

(3) The predicted strengths are compared with the corresponding measured strengths and the mean variance thereby calculated for a given set of T-curve parameters.

(4) The T-curve parameters are incremented and the calculation of the variance repeated, using a matrix search routine. The increments in the search variables were 0.05 MPa  $m^{1/2}$  for the toughness parameters  $T_0$  and  $T_\infty$  and 5  $\mu\text{m}$  for the dimension parameters  $d$  and  $c^*$ .

(5) The set of T-curve parameters yielding the minimum residual variance is selected.

## IV. RESULTS

The materials analyzed in this study are listed in Table I, along with their Young's modulus, hardness, grain size, and minor phase percentage. Previously published<sup>1,3,4,11</sup> indentation-strength data for these materials was used for the T-curve deconvolutions. [Some data were removed from the original  $\sigma_m(P)$  data sets at large indentation loads, where the influence of secondary lateral cracking was suspected to have significantly decreased the magnitude of the residual stress intensity factor.<sup>20</sup>] The resultant parameter evaluations are given in Table II.

Our first exercise was to select a fixed value of the exponent  $m$  for the T-curve evaluations. Accordingly a preliminary analysis of the  $\sigma_m(P)$  data for two materials displaying particularly strong T-curve influences in their strength responses, namely the VI1 and VI2 aluminas, was carried out. Figure 4 shows the minimum resid-

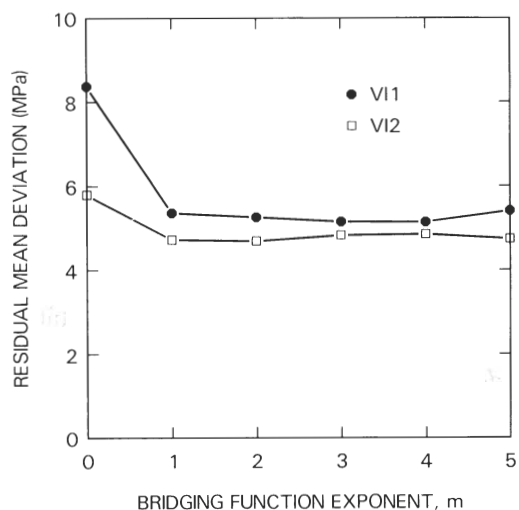


FIG. 4. The residual mean deviation between fitted and measured indentation-strength functions versus bridging function exponent  $m$  for the VI aluminas. Note the relative insensitivity for  $m \geq 1$ .

ual mean deviation as a function of  $m$  for these materials. The deviation for both materials is greatest at  $m = 0$  but thereafter at  $m \geq 1$  is insensitive to the choice of exponent. The value somewhat arbitrarily chosen for this study was  $m = 2$  in accord with that adopted in the concrete literature.<sup>10</sup>

To illustrate the procedure and at the same time to gain valuable insight into the crack evolution to failure let us focus now on just two of the listed alumina materials in Table I, VI2 and AD96. Figure 5 shows the strength versus indentation load data for these materials.<sup>1</sup> The data points in this figure represent means and standard deviations of approximately ten strength tests at each indentation load. The solid lines are the best fits [Eqs. (1), (6), and (11)] to the data. The dashed lines represent  $T_0$ - and  $T_\infty$ -controlled limits [Eqs. (12) and (13)]. As can be seen, the fitted curves smoothly intersect the  $T_\infty$ -controlled limit at large indentation loads, this tendency being greater for the AD96 material. This smooth connection is a reflection of our choice of  $m$  above; for  $m < 2$  the  $\sigma_m(P)$  curve intersects the  $T_\infty$  limit with a discontinuity in slope. At intermediate indentation loads the strengths tend to a plateau level, more strongly for the VI2 material. In line with our contention that this plateau is associated with a strong microstructural influence we might thus expect the VI2 material to exhibit a more pronounced T curve. The larger separation of the  $T_0$ - and  $T_\infty$ -controlled limits for the VI2 material in Fig. 6 supports this contention. Finally, at small indentation loads the strengths cut off abruptly at the  $T_0$ -controlled limit, corresponding to the case

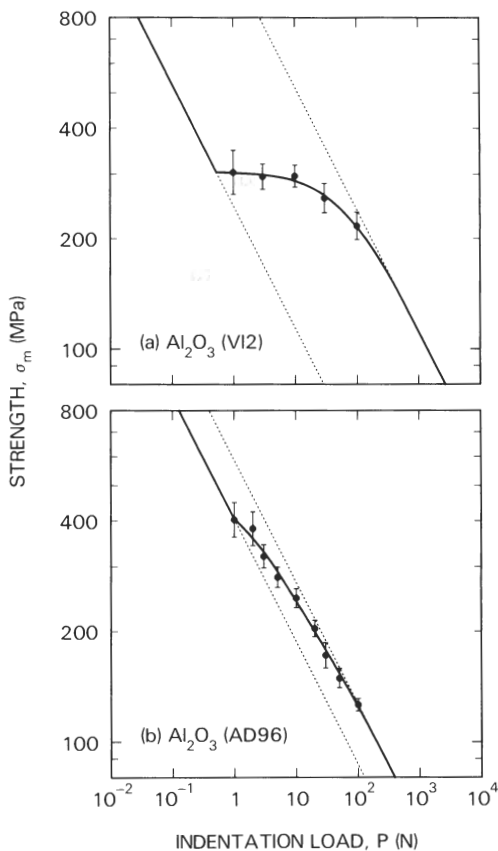


FIG. 5. Indentation-strength data fits for the VI2 and AD96 aluminas. Note the relatively pronounced plateau for the VI2 material, indicative of a strong T-curve influence. Oblique dashed lines are  $T_0$ - and  $T_\infty$ -controlled limiting solutions.

TABLE I. Materials analyzed in this study.

Material		Young's modulus $E$ /GPa	Hardness $H$ /GPa	Grain size $\mu\text{m}$	Minor phase %	Ref.
Alumina	VI1	393	19.1	20	0.1	1
	VI2	393	19.0	41	0.1	1
	AD999	386	20.1	3	0.1	1
	AD96	303	14.1	11	4	...
	AD90	276	13.0	4	10	1
	F99	400	16.1	11	1	1
	HW	206	11.7	28	0.3	1
	Sapphire	425	21.8	...	...	1
Glass-ceramics	SL1	87.9	4.4	1.2	33	1,3
	SL2	87.9	4.3	1.9	22	1,3
	SL3	87.9	4.8	2.3	20	1,3
	Macor	64.1	2.0	17	50	4
	Pyroceram	108	8.4	1	...	4
Barium titanate	CH(cub.)	123	5.9	7	1	11
	CH(tet.)	123	5.9	7	1	11

where the crack intersects no bridges prior to unlimited instability.

Figures 6 and 7 show the corresponding equilibrium  $\sigma_a(c)$  and  $T(c)$  functions that underlie the curve fits in Fig. 5. The  $\sigma_a(c)$  responses are plotted for several indentation loads, embracing the data range covered in the indentation-strength experiments (e.g., Fig. 5). The most distinctive feature of these curves is that at low indentation loads, where the initial crack size is somewhat smaller than the first barrier distance  $d$ , there are two maxima, most notably in the VI2 material. The first maximum, at  $c < d$ , is a pure manifestation of the crack stabilization due to the residual contact stress term [Eq. (11)].<sup>19</sup> The second maximum, at  $c > d$ , results from the additional, abrupt stabilization associated with the microstructural closure forces. Of the two maxima, it is the greater that determines the strength. Thus at very low  $P$  (corresponding to region I in Fig. 3) the first maximum wins, and the instability takes the crack system to failure without limit (e.g., the  $P = 0.1$  N curves for both the VI2 material in Fig. 6 and the AD96 material in Fig. 7). At intermediate  $P$  (region II in Fig. 3) the second maximum becomes dominant, in which case the

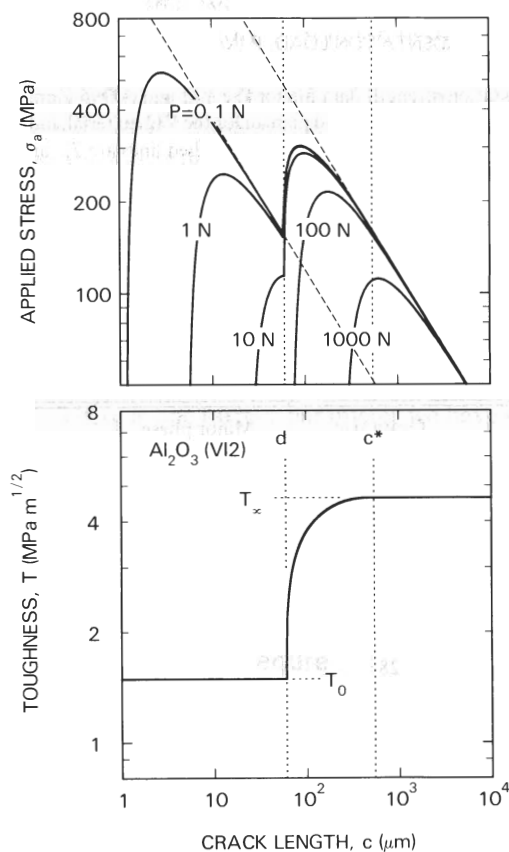


FIG. 6. (a) Applied stress versus equilibrium crack length at different indentation loads and (b) corresponding T curve, for VI2 alumina, as derived from the indentation-strength data in Fig. 5.

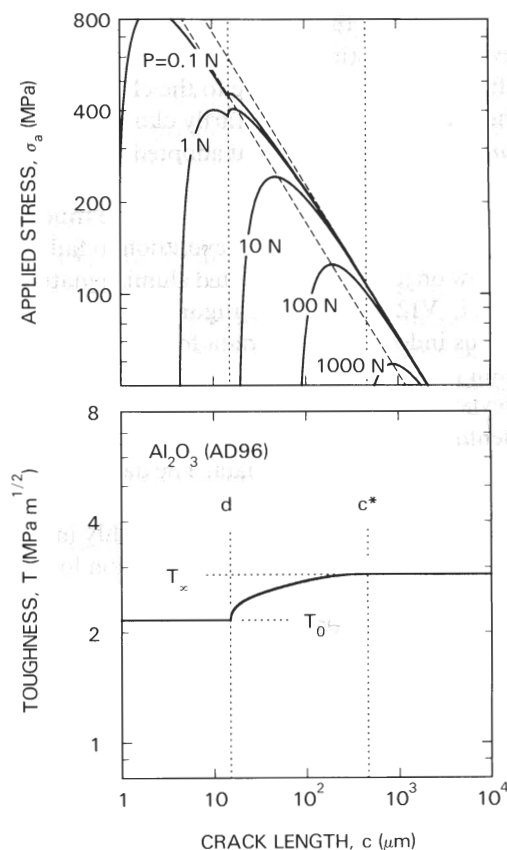


FIG. 7. (a) Applied stress versus equilibrium crack length and (b) corresponding T curve, for AD96 alumina.

crack arrests before failure can ensue (e.g., the  $P = 1$  N curves in Figs. 6 and 7). Note that the second maximum for the VI2 alumina occurs at  $\approx 100 \mu\text{m}$ , consistent with abrupt initial jumps of 2–5 grain diameters reported by Swanson *et al.* At large  $P$  (region III in Fig. 3) the curves tend more and more to a single pronounced maximum, as we once more enter a region of invariant toughness. In all cases, however, we note that the stabilizing influences of the residual and microstructural stress intensity factors render the strength insensitive to the initial crack length.

It is in the transition region, region II, where the form of the T curve most strongly influences the crack stability and strength properties. The T curve for the VI2 alumina rises more steeply than that for the AD96 alumina. The difference in responses for the two materials may be seen most clearly in the  $\sigma_a(c)$  curves for  $P = 10$  N, Figs. 6 and 7. In VI2 alumina the restraint exerted on the crack by the interfacial bridges is apparently much stronger than in AD96. We note that the indentation-strength curves in Fig. 5 may be seen as “rotated” versions of the T curves in Figs. 6 and 7.

A word is in order here concerning the “sensitivity” of the parameter evaluation to the range of data. Figure

8 shows the deconvoluted T curves for the VI2 material with individual data points at either end of the indentation load range deliberately omitted from the base data in Fig. 5(a). When data are "lost" from the large  $P$  end, the high  $T(c)$  part of the curve is most affected; similarly, for data omissions at the small  $P$  end, the low  $T(c)$  part of the curve is most affected. We may regard the curve shifts in Fig. 8 as characterizing the *systematic* uncertainty in our parameter evaluations, just as the mean residual deviation in the regression procedure characterizes the *random* uncertainty. We note that it is those parameters that control the upper and lower bounds of the T curve that are subject to the greatest uncertainty, since it is in these extreme regions (especially in the  $T_0$ -controlled region) where indentation-strength data are most lacking. The central portions of the T curves in Fig. 8 are not altered substantially by the deletion of strength data.

Subject to the above considerations, we may now usefully summarize the relative T-curve behavior for the remainder of the materials listed in Table II. The T curves are shown in Figs. 9–11 for each of the material types, aluminas, glass-ceramics, and barium titanates. Special attention may be drawn to the fact that the curves for the microstructurally variant materials in each of these composite plots tend to cross each other. We note in particular that the curves for the polycrystalline aluminas in Fig. 9 cross below that for sapphire at small crack sizes, consistent with earlier conclusions that the intrinsic polycrystal toughness ( $T_0$ ) is governed by grain boundary properties.<sup>1</sup>

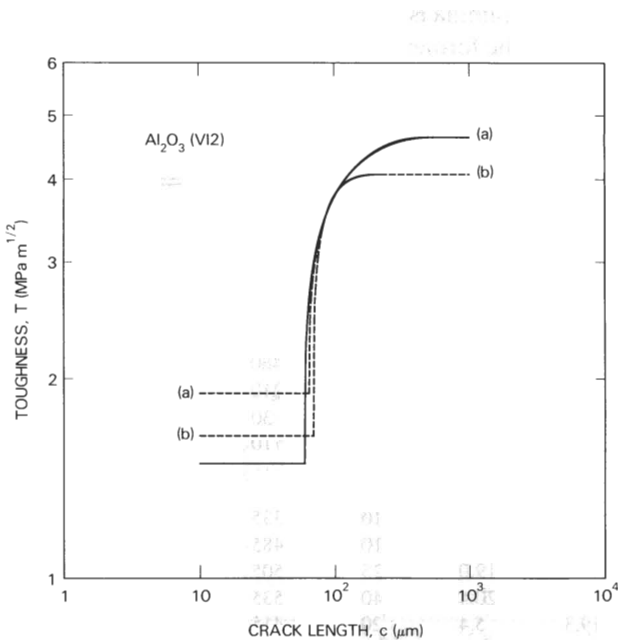


FIG. 8. Deconvoluted T-curve plots for the VI2 alumina using full indentation-strength data set from Fig. 5(a) (solid line) and same data truncated (dashed lines) by removal of extreme data points at (a) low  $P$  and (b) high  $P$ .

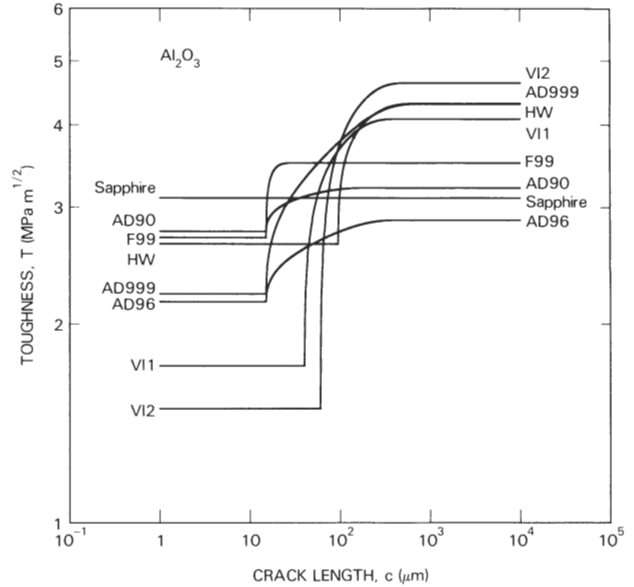


FIG. 9. Composite plot of the deconvoluted T curves for the alumina materials.

## V. DISCUSSION

We have considered a fracture toughness model based on an independently verified interface restraint mechanism<sup>8,9</sup> for explaining the microstructural effects previously reported in indentation/strength data.<sup>1-4</sup> A key feature of our modeling is the strong stabilizing effect of grain-scale ligamentary bridges on the stability conditions for failure. (In this sense our explanation differs somewhat from that originally offered by us in

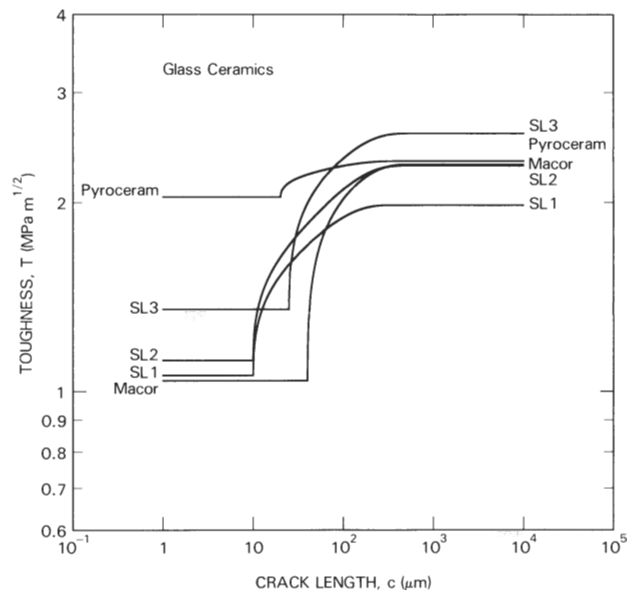


FIG. 10. Composite plot of the deconvoluted T curves for the glass-ceramic materials.

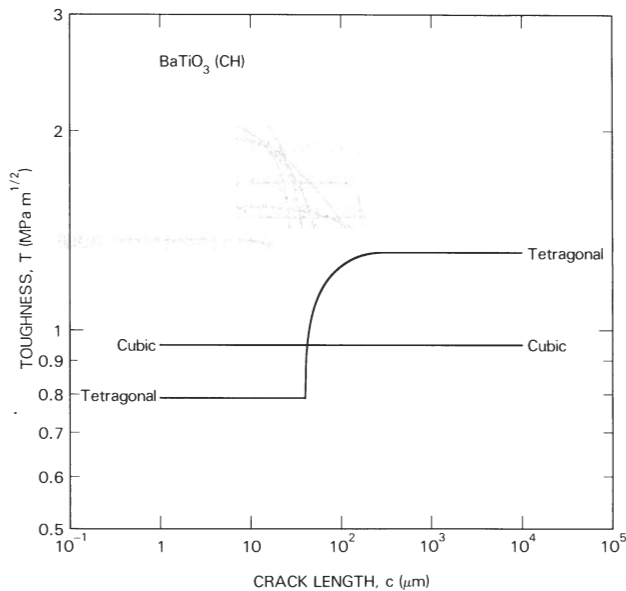


FIG. 11. Composite plot of the deconvoluted T curves for the barium titanate material.

Ref. 1, where it was tacitly suggested that the microstructural influence might be represented as a *positive decreasing function of crack size*. The distinction between negative increasing and positive decreasing  $K_{\mu}$  functions is not easily made from strength data alone.) Although the earlier experimental observations used to establish the model<sup>18</sup> were based almost exclusively on one particular alumina ceramic,<sup>1</sup> our own detailed crack observations, and those of others, strongly suggest that the model is generally applicable to other nontransforming ceramics; the discontinuous primary crack traces

characteristic of the bridging process have since been observed in other aluminas,<sup>12,21</sup> glass-ceramics,<sup>12,21,22</sup> SiC ceramics,<sup>23</sup> and polymer cements.<sup>21</sup> The fact that the resultant strength equations from the model can be fitted equally well to all the materials examined in the present study serves to enhance this conviction.

A characteristic feature of the failure properties of the materials with pronounced T curves (e.g., VI2 alumina) is the relative insensitivity of the strength to initial flaw size. This is a vital point in relation to structural design. Materials with strong T-curve responses have the quality of flaw tolerance. Ideally, it would seem that one should seek to optimize this quality. Associated with this tolerance is an enhanced crack stability. This offers the potential detection of failures. On the other hand, there is the indication that such benefits may only be wrought by sacrificing high strengths at small flaw sizes. This tendency is clearly observed in the way the strength curves cross each other in Figs. 7–9 in Ref. 1 (corresponding to crossovers seen here in the T curves, Figs. 9–11). In other words, the designer may have to practice the gentle art of compromise.

We reemphasize that the T-curve parameters derived from the strength data (Table II) are elements of curve fitting and are subject to systematic as well as to the usual random uncertainties. Since any four of these parameters are independent, our numerical procedure, regardless of “goodness of fit,” cannot be construed as “proof” of our model. Nevertheless, we may attach strong physical significance to these parameters. For example, the relatively large values of  $\Gamma_1$  and  $c^*$  for the VI materials relative to the corresponding parameters for the F99 alumina is a clear measure of a greater T-curve effect in the former. More generally, the aluminas with

TABLE II. T-curve parameters derived from strength data for  $m = 2$  (from Refs. 1, 3, 4, 11).

Material	$T_0$ (MPa m <sup>1/2</sup> )	$T_{\infty}$ (MPa m <sup>1/2</sup> )	$\Gamma_0$ (J m <sup>-2</sup> )	$\Gamma_1$ (J m <sup>-2</sup> )	$d$ ( $\mu$ m)	$c^*$ ( $\mu$ m)	$\sigma^*$ (MPa)	$u^*$ ( $\mu$ m)
VI1	1.73	4.08	3.8	10.4	40	420	280	0.11
VI2	1.49	4.63	2.8	11.8	60	540	328	0.11
AD999	2.22	4.30	6.4	12.0	15	715	188	0.19
AD96	2.16	2.87	8.5	5.6	15	460	80	0.19
AD90	2.76	3.21	13.8	4.6	15	210	75	0.18
F99	2.70	3.50	9.1	5.4	15	30	405	0.04
HW	2.64	4.31	16.9	21.4	95	710	153	0.42
Sapphire	3.10	3.10	11.3	0	...	...	...	...
SL1	1.06	1.98	6.4	11.2	10	335	122	0.27
SL2	1.12	2.29	7.1	15.0	10	485	129	0.35
SL3	1.35	2.58	10.4	19.0	25	505	133	0.43
Macor	1.04	2.30	8.4	20.4	40	535	132	0.46
Pyroceram	2.04	2.33	19.3	5.4	20	415	35	0.48
CH(cub.)	0.95	0.95	3.7	0	...	...	...	...
CH(tet.)	0.79	1.35	2.5	3.6	40	330	70	0.14

glassy phases at their grain boundaries,<sup>24</sup> or with smaller grain size (Tables I and II) have relatively low toughness indices,  $\Gamma_1/\Gamma_0$ , indicating that there is some kind of trade-off between macroscopic and microscopic toughness levels, and that this trade-off is controlled by the microstructure. We note also that the maximum stress-separation range parameters  $u^*$  for the materials are in the range 0.1–0.4  $\mu\text{m}$ , consistent with crack opening displacement observations at the bridging sites.<sup>8,12,21–23</sup> We thus suggest that such parameters could serve as useful guides to materials processors, for tailoring materials with desirable, predetermined properties, especially with regard to grain boundary structure.

Mention was made in Sec. IV of the sensitivity of the parameter evaluations to the available data range. This has implications concerning conventional, large-crack toughness measurements. To investigate this point further we plot in Fig. 12 the  $T_\infty$  values determined here against those measured independently by macroscopic techniques. The degree of correlation in this plot would appear to lend some confidence to our fitting procedure (and to our *a priori* choices for the parameters  $\psi$  and  $\chi$ ). Since most of our strength data tend to come from regions toward the top of the T curve we should perhaps not be too surprised at this correlation.

Finally, we may briefly address the issue of test specimen geometry in connection with the accuracy of the parameter evaluations. It has been argued elsewhere<sup>9</sup> that test specimen geometry can be a crucial factor in the T-curve determination. It might be argued, for

instance, that “superior” parameter evaluations could be obtained from larger crack geometries, particularly the  $c^*$ ,  $T_\infty$  parameters. However, the indentation methodology takes us closer to the strengths of specimens with natural flaws, in particular to the  $T_0$ -controlled regions (notwithstanding our qualifying statements earlier concerning this parameter), so that the present evaluations may be more appropriate for designers.

## VI. CONCLUSIONS

(1) An independently confirmed ligament bridging model is used as the basis for analyzing observed indentation-strength data for a wide range of polycrystalline ceramic materials.

(2) Those materials with pronounced T curves show the qualities of “flaw tolerance” and enhanced crack stability.

(3) A fracture mechanics treatment of the indentation fracture system with microstructure-associated factors incorporated allows for the (numerical) deconvolution of toughness/crack-length (T-curve) functions from these data.

(4) Comparisons within a range of aluminas suggest that those materials with “glassy” grain boundaries and smaller grain size have less pronounced T curves than those with “clean” boundaries.

(5) The indentation-strength technique and the toughness parameters deriving from it should serve as useful tools for the development of ceramic materials with predetermined properties, especially with respect to grain boundary structure and chemistry.

## ACKNOWLEDGMENTS

The authors thank C. Thompson for assistance with some of the computer programs used in this work.

Funding for the National Bureau of Standards component of this work was provided by the Air Force Office of Scientific Research.

## APPENDIX: EVALUATION OF $\psi$ AND $\chi$

Here we derive numerical values for the dimensionless parameters  $\psi$  and  $\chi$  characterizing the crack geometry and the intensity of the residual contact stress, respectively. The choices for these should yield agreement between measured strength and toughness properties of homogeneous materials with no measurable T-curve behavior (i.e.,  $K_\mu = 0$ ,  $T = T_0 = T_\infty$ ).

We begin with the geometrical  $\psi$  term, which is assumed to be material independent. From the applied stress (strength)  $\sigma_m$  and crack length  $c_m$  at the instability point of an indentation, we can show that<sup>25</sup>

$$\psi = 3T/4(\sigma_m c_m^{1/2}). \quad (\text{A1})$$

Measurements of  $\sigma_m c_m^{1/2}$  for several homogeneous mate-

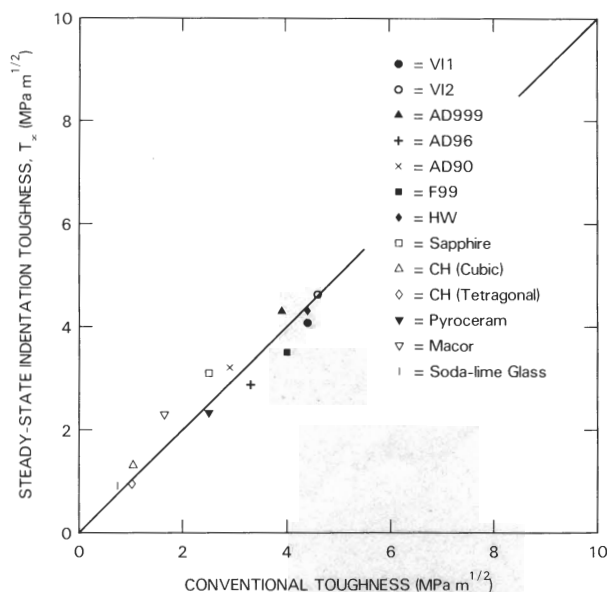


FIG. 12. Plot of  $T_\infty$  (Table II) as a function of independently measured toughness using conventional macroscopic specimens.

rials confirm that Eq. (A1) describes the toughness/instability properties<sup>25,26</sup> for  $\psi = 1.24$ . We note that this is very close to the value of 1.27 calculated by finite element analyses of semicircular cracks in surfaces of bend specimens.<sup>27</sup>

For the  $\chi$  term we turn to Ref. 13, where it is shown that

$$\chi = \xi(E/H)^{1/2}, \quad (\text{A2})$$

where  $\xi$  is a material-independent constant. With this result Eq. (12) may be rewritten as<sup>28</sup>

$$T_0 = \eta(E/H)^{1/8}(\sigma_m^0 P^{1/3})^{3/4}, \quad (\text{A3})$$

where

$$\eta = (256\psi^{1/3}\xi/27)^{1/4} \quad (\text{A4})$$

is another material-independent constant. From measurements of  $\sigma_m^0 P^{1/3}$  for a similar range of homogeneous material we obtain  $\eta = 0.52$ .<sup>26</sup> Hence eliminating  $\xi$  from Eqs. (A2) and (A4) yields

$$\chi = 27\eta^4(E/H)^{1/2}/256\psi^3, \quad (\text{A5})$$

which gives  $\chi = 0.0040(E/H)^{1/2}$ .

## REFERENCES

- <sup>1</sup>R. F. Cook, B. R. Lawn, and C. J. Fairbanks, *J. Am. Ceram. Soc.* **68**, 604 (1985).
- <sup>2</sup>R. F. Cook, B. R. Lawn, and C. J. Fairbanks, *J. Am. Ceram. Soc.* **68**, 616 (1985).
- <sup>3</sup>R. F. Cook, S. W. Freiman, and T. L. Baker, *Mater. Sci. Eng.* **77**, 199 (1986).
- <sup>4</sup>C. J. Fairbanks, B. R. Lawn, R. F. Cook, and Y.-W. Mai, in *Fracture Mechanics of Ceramics*, edited by R. C. Bradt, A. G. Evans, D. P. H. Hasselman, and F. F. Lange (Plenum, New York, 1986), Vol. 8, pp. 23-37.
- <sup>5</sup>H. Hübner and W. Jillek, *J. Mater. Sci.* **12**, 117 (1977).
- <sup>6</sup>R. Knehans and R. Steinbrech, *J. Mater. Sci. Lett.* **1**, 327 (1982).
- <sup>7</sup>R. Steinbrech, R. Knehans, and W. Schaawächter, *J. Mater. Sci.* **18**, 265 (1983).
- <sup>8</sup>P. L. Swanson, C. J. Fairbanks, B. R. Lawn, Y.-W. Mai, and B. R. Hockey, *J. Am. Ceram. Soc.* **70**, 279 (1987).
- <sup>9</sup>Y.-W. Mai and B. R. Lawn, *Annu. Rev. Mater. Sci.* **16**, 415 (1986).
- <sup>10</sup>Y.-W. Mai and B. R. Lawn, *J. Am. Ceram. Soc.* **70**, 289 (1987).
- <sup>11</sup>R. F. Cook, S. W. Freiman, B. R. Lawn, and R. C. Pohanka, *Ferroelectrics* **50**, 267 (1983).
- <sup>12</sup>P. L. Swanson, in *Advances in Ceramics* (in press).
- <sup>13</sup>B. R. Lawn, A. G. Evans, and D. B. Marshall, *J. Am. Ceram. Soc.* **63**, 574 (1980).
- <sup>14</sup>D. R. Clarke, B. R. Lawn, and D. H. Roach, in Ref. 4, pp. 341-350.
- <sup>15</sup>I. N. Sneddon, *Proc. R. Soc. London Ser. A* **187**, 229 (1946).
- <sup>16</sup>B. R. Lawn and T. R. Wilshaw, *Fracture of Brittle Solids* (Cambridge U. P., Cambridge, 1975).
- <sup>17</sup>D. B. Marshall, B. N. Cox, and A. G. Evans, *Acta Metall.* **33**, 2013 (1985).
- <sup>18</sup>D. B. Marshall and B. R. Lawn, *J. Mater. Sci.* **14**, 2001 (1979).
- <sup>19</sup>D. B. Marshall, B. R. Lawn, and P. Chantikul, *J. Mater. Sci.* **14**, 2225 (1979).
- <sup>20</sup>R. F. Cook and D. H. Roach, *J. Mater. Res.* **1**, 589 (1986).
- <sup>21</sup>R. F. Cook (unpublished work).
- <sup>22</sup>K. T. Faber and A. G. Evans, *Acta Metall.* **31**, 577 (1983).
- <sup>23</sup>K. T. Faber and A. G. Evans, *J. Am. Ceram. Soc.* **66**, C-94 (1983).
- <sup>24</sup>S. L. Fortner (unpublished work).
- <sup>25</sup>R. F. Cook and B. R. Lawn, *J. Am. Ceram. Soc.* **66**, C-200 (1983).
- <sup>26</sup>R. F. Cook, Ph.D. thesis, University of New South Wales, Australia, 1985.
- <sup>27</sup>J. C. Newman and I. S. Raju, *Eng. Fract. Mech.* **15**, 185 (1981).
- <sup>28</sup>P. Chantikul, G. Anstis, B. R. Lawn, and D. B. Marshall, *J. Am. Ceram. Soc.* **64**, 539 (1981).